# 8. Planatary boundary layer*

## 8.1 Introduction

The layer adjacent to the earth's surface is called the planetary boundary layer (PBL), where turbulent motions are dominant in redistributing sensible heat, moisture and momentum in the vertical direction. The atmosphere above the PBL is called the free atmosphere. We idealize in modeling the PBL that turbulent fluxes are completely absent in the free atmosphere except in the cumulus ensembles. This simplification introduces the exsistence of gaps in physical variables at the top of the PBL.

Variety of informations of the earth's surface is conveyed to the free atmosphere through the PBL. Therefore the depth and the structure of the PBL, and thus the turbulent fluxes of energy and momentum in it are greatly controlled by the surface conditions as well as by synoptic conditions in the free atmosphere.

The PBL model of the MRI•GCM-I is based on the model by Randall and Arakawa described in AM and by Randall (1976) with minor changes in several respects. The model predicts the depth and the mean structure of the PBL by taking account of the interactions with large-scale circulations as well as with the surface conditions. It also interacts with a sophisticated parameterization of cumulus convection described in Chapter 7, which is based on the theory of Arakawa and Schubert (1974). The possible existence of stratus or stratocumulus clouds within the PBL is also taken account of in the diagnostic determination of the turbulent fluxes.

Governing equations for the large-scale circulation are described in 8.2. The diagnostic determination of turbulent fluxes and the entrainment rate at the top of the PBL is given in 8.3. The treatment of the stratus layer is given in 8.4 and the vertical interpolation scheme and numerical procedures are given in 8.5 and 8.6, respectively. Some examples of the model performance are shown in the Appendix 8.1.

## 8.2 Governing equations for the large-scale circulation

The conservation of mass in the $\sigma$-coordinate system is given by (0.14). Let $\sigma_B$ and $\delta\sigma_m$ $(=1-\sigma_B)$ be the top and the depth of the PBL in $\sigma$-space respectively. Vertical integration of

---

* This chapter is prepared by T. Tokioka.

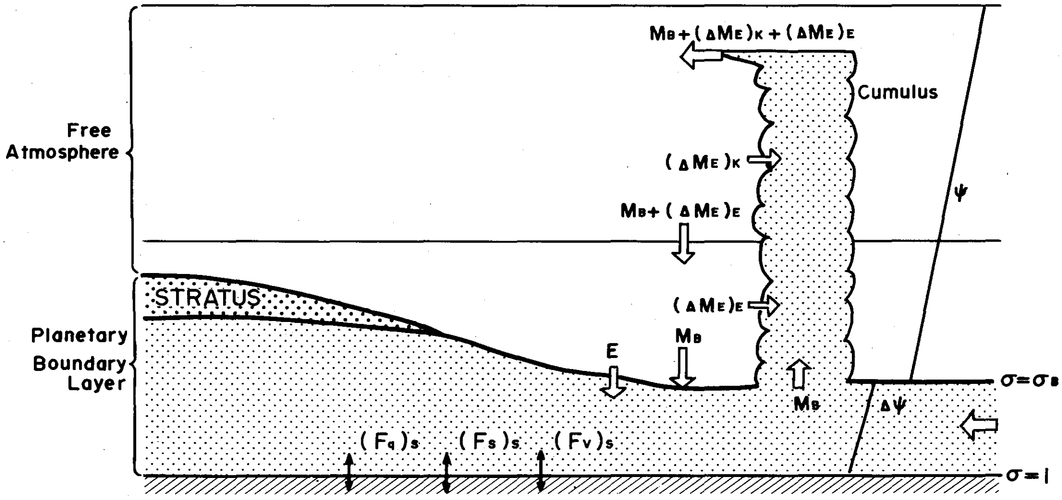


Fig. 8.1 Schematical figure of the PBL model in the GCM. The PBL interacts with the free atmosphere, with the ensemble of cumulus and with the lower surface of the atmosphere. White arrows show mass flows related to the mass budget of the PBL.

(0.14) from $\sigma=\sigma_B$ to 1 results in the following equation:

$$\frac{\partial}{\partial t}(\pi\delta\sigma_m)+\nabla\cdot(\pi\delta\sigma_m\mathbf{v}_m)-g(E-M_B)=0 \tag{8.1}$$

where

$$E-M_B=-\frac{\pi}{g}\left(\frac{\partial\sigma_B}{\partial t}+\mathbf{v}_B\cdot\nabla\sigma_B-\dot{\sigma}_B\right) \tag{8.2}$$

and

$$\mathbf{v}_m=\frac{1}{\delta\sigma_m}\int_{\sigma_B}^{1}\mathbf{v}d\sigma$$

The right hand side of (8.2) indicates the net downward mass flux across the PBL top, and the term is decomposed into two parts, *i. e.* E and $M_B$, for the later convenience. E is the rate at which mass is entrained into the PBL from the free atmosphere, and $M_B$ is the rate at which mass is lost from the PBL into the cumulus cloud ensembles (see Fig. 8.1). If we integrate (0.14) from the level just above the PBL $\sigma=\sigma_{B+}$ to $\sigma=\sigma_B$, then we get

$$\pi\Delta(\mathbf{v}\cdot\nabla\sigma_B-\dot{\sigma})=0 \tag{8.3}$$

where $\Delta\psi$ indicates a gap in the quantity $\psi$ at the PBL top.

The diabatic term $\pi Q$ in the thermodynamic equation (0.26) is expressed as

$$\pi Q = g\frac{\partial}{\partial\sigma}(F_S + R) + \pi(LC + Q_S) \tag{8.4}$$

where $F_s$ is the upward turbulent flux of sensible heat; R, the net upward flux of radiation; and C is the net condensation rate due to processes other than cumulus convection. The heating due to a possible ensemble of cumulus clouds is expressed as $Q_S$. If we integrate (0.28) from $\sigma = \sigma_{B+}$ to $\sigma = \sigma_B$, we get

$$(F_S)_B - \Delta R + \frac{\pi}{g}\int_{\sigma_{B+}}^{\sigma_B} LC\, d\sigma + Ec_p\Delta T = 0 \tag{8.5}$$

where use has been made of (8.2) and (8.3), and the following assumption

$$\pi\int_{\sigma_{B+}}^{\sigma_B} Q_S d\sigma = -g\int_{\sigma_{B+}}^{\sigma_B} M\frac{\partial s}{\partial\sigma}d\sigma = gM_Bc_p\Delta T$$

$M_B$ is the cumulus ensemble mass flux at $\sigma = \sigma_B$, and s indicates dry static energy, $c_pT + \phi$. The second and the third terms of (8.5) are zero except when the upper portion of the PBL is filled with stratus (cloud-topped PBL).

In a non-precipitable moist process, both moist static energy h $(= s + Lq)$ and total water substance $q_w$ $(= q + l)$, where $l$ is the mixing ratio of liquid water, are conserved. By analogy with (8.5), we have

$$(F_h)_B - \Delta R + E\Delta h = 0 \tag{8.6}$$

and

$$(Fq_w)_B + E\Delta q_w = 0 \tag{8.7}$$

where $(F_h)_B$ and $(Fq_w)_B$ are the vertical turbulent fluxes of h and $q_w$ at the PBL top. From (8.5), (8.6) and (8.7), we get

$$-\frac{\pi}{g}\int_{\sigma_{B+}}^{\sigma_B} LC d\sigma = L[(F_l)_B - El_B] \tag{8.8}$$

where $(F_l)_B$ is the vertical turbulent flux of $l$ at $\sigma = \sigma_B$.

In a similar way, we obtain

$$\frac{\pi}{g}\int_{\sigma_{C+}}^{\sigma_{C-}} LC d\sigma = LF_{lC+} \tag{8.9}$$

where $\sigma_{C\pm}$ indicate the positions immediately above and below the stratus cloud base.

From the momentum equations, we obtain

$$(\mathbf{F}_v)_B + E\Delta\mathbf{v} = 0 \tag{8.10}$$

where $(\mathbf{F}_v)_B$ indicates vertical flux vector of horizontal momentum at $\sigma = \sigma_B$.

Here we introduce a new coordinate $\sigma' = \sigma - \sigma_B$. The PBL top is just $\sigma' = 0$ in this coordinate. With use of the relation

$$\left(\frac{\partial}{\partial \xi}\right)_{\sigma} = \left(\frac{\partial}{\partial \xi}\right)_{\sigma'} - \frac{\partial \sigma_B}{\partial \xi}\frac{\partial}{\partial \sigma} \tag{8.11}$$

where $\xi$ is either time or horizontal coordinate, we can rewrite thermodynamic equation (0. 26), conservation equation of total water substance (0.28) and momentum equation (0.23). From those equations, we can derive following jump equations:

$$c_p \pi \frac{\partial \Delta T}{\partial t} = -c_p \left[ \underline{\Delta(\pi \mathbf{v} \cdot \nabla_{\sigma'} T)} + g(E - M_B)\Delta\left(\frac{\partial s}{\partial \sigma}\right) \right] + \pi \Delta \left[ \left( \frac{\partial p_B}{\partial t} + \mathbf{v} \cdot \nabla p_B \right) \alpha \right]$$
$$+ g\left[ \Delta\left(\frac{\partial R}{\partial \sigma}\right) - \left(\frac{\partial F_s}{\partial \sigma}\right)_B \right] + \pi \Delta (LC + Q_s) \tag{8.12}$$

$$\pi \frac{\partial \Delta q_w}{\partial t} = -\underline{\Delta(\pi \mathbf{v} \cdot \nabla_{\sigma'} q_w)} - g(E - M_B)\Delta\left(\frac{\partial q_w}{\partial \sigma}\right) - \left[ \Delta\left(\frac{\partial r}{\partial \sigma}\right) + g\left(\frac{\partial F q_w}{\partial \sigma}\right)_B \right] \tag{8.13}$$

$$\pi \frac{\partial \Delta \mathbf{v}}{\partial t} = -\underline{\nabla[\pi \mathbf{v} \cdot \nabla_{\sigma'} \mathbf{v}]} - g(E - M_B)\Delta\left(\frac{\partial \mathbf{v}}{\partial \sigma}\right) - \pi \Delta \alpha \nabla p_B$$
$$- \pi \left[ f\mathbf{k} \times \Delta \mathbf{v} + \frac{\tan\varphi}{a} \mathbf{k} \times \Delta(u\mathbf{v}) \right] - g\left(\frac{\partial \mathbf{F}_v}{\partial \sigma}\right)_B \tag{8.14}$$

where r is the downward flux of water substance due to precipitation.
In deriving (8.12), use has been made of

$$\omega_B = \frac{\partial p_B}{\partial t} + \mathbf{v}_B \cdot \nabla p_B + g(E - M_B) = \omega_{Bt} - \Delta \mathbf{v} \cdot \nabla p_B$$

It is pointed out that the balance between the term $\pi \Delta \alpha \nabla p_B$ and $\pi f\mathbf{k} \times \Delta \mathbf{v}$ in (8.14) may be understood as an extention of Margules' relation to the wind and density discontinuities at the PBL top.

### 8.3 Diagnostic determination of the entrainment rate at the top of the PBL and of turbulent fluxes

Turbulent kinetic energy equation in the planetary boundary layer may be written as

$$\frac{dq^2}{dt} + \frac{\partial}{\partial z}\overline{w'\left(\frac{p'}{\rho} + q^2\right)} = \frac{\tau}{\rho} \cdot \frac{\partial \mathbf{v}}{\partial z} + \frac{g}{\bar{s}_v}\overline{w' s_v'} - \delta \tag{8.15}$$

where $q^2$ is turbulent kinetic energy density, w is vertical velocity, $\tau$ is stress ($=\rho\overline{\mathbf{v}'w'}$), $\rho$ is density, $\delta$ is the dissipation rate of turbulent kinetic energy, and $s_v$ is the virtual dry static energy ($= s + \epsilon L\,(0.61q - l)$, $\epsilon = c_pT/L$). Dash is an indicator of turbulent quantity and a superior bar is an average operation. In deriving (8.15), turbulence is assumed to be homogeneous in the horizontal direction.

We integrate (8.15) from the surface ($z=0$) to the top of the PBL ($z=z_B$). Then the left hand side of (8.15) may be approximated as

$$\rho z_B \frac{Dq_m{}^2}{Dt} + \rho E q_m{}^2 \tag{8.16}$$

where

$$\frac{D}{Dt} = \frac{\partial}{\partial t} + \mathbf{v}_m \cdot \nabla$$

The subscript "m" indicates that the value is a representative value in the PBL.

The first term on the r.h.s. of (8.15) is the generation of turbulent kinetic energy by the vertical wind shear, which is considered to be large both near the surface and the PBL top where the vertical wind shear is usually large. Therefore we introduce the following approximation,

$$\int_0^{z_B} \rho \cdot \frac{\tau}{\rho} \cdot \frac{\partial \mathbf{v}}{\partial z} dz = a_1 \rho u_*{}^3 + a_2 \rho \mid \Delta \mathbf{v} \mid ^3 \tag{8.17}$$

where $u_*$ is the friction velocity. $a_1$ and $a_2$ are constants yet undetermined.

The second term on the r.h.s. of (8.15) is the generation of the turbulent kinetic energy due to buoyancy flux. The buoyancy flux, based on its definition, is related to the turbulent flux of h and $q_w$ as follows:

$$\overline{w's_v'} = \begin{cases} (1+0.61\bar{q})\overline{w'h'} - (1-0.61\bar{\epsilon}+0.61\bar{q})L\overline{w'q_w'} & : \text{outside clouds} \\ \left(\alpha + \dfrac{0.61\bar{q}-\bar{l}}{1+\gamma}\right)\overline{w'h'} - \bar{\epsilon}L\overline{w'q_w'} & : \text{inside clouds} \end{cases}$$

where

$$h = s + Lq$$

$$q_w = q + l$$

$$s_v = s + \epsilon L(0.61q - l) \tag{8.18}$$

$$\alpha = (1+1.61\gamma\epsilon)/(1+\gamma)$$

$$\gamma = \frac{L}{c_p}\left(\frac{\partial q^*}{\partial T}\right)_p$$

$$\epsilon = c_p T_o / L$$

$q^*$ : saturation mixing ratio of water vapour

Here, we introduce the following assumption:

Turbulent fluxes within the PBL tend to mix moist static energy h and the mixing ratio of total water substance $q_w$, *i.e.* the turbulent flux profile of both h and $q_w$ is linear with height in the PBL.

Then we have a similar result to the one obtained by Deardorff (1976),

$$\int_0^{z_B} \rho \frac{g}{\bar{s}_v} \overline{w's_v'} dz = \frac{g z_B}{(\bar{s}_v)_m} (A - \rho EB) \tag{8.19}$$

where

$$A = \mu_1 (F_h)_s + \mu_2 \Delta R - \mu_3 L (F_q)_s$$

$$B = \mu_2 \Delta h - \mu_4 L \Delta q_w$$

$$\mu_1 = \frac{1}{2}(1 + 0.61\bar{q}) + \frac{1}{2}(\alpha + \frac{0.61\bar{q} - \bar{l}}{1+\gamma} - 1 - 0.61\bar{q})(1-\xi)^2$$

$$\mu_2 = \frac{1}{2}(1 + 0.61\bar{q}) + \frac{1}{2}(\alpha + \frac{0.61\bar{q} - \bar{l}}{1+\gamma} - 1 - 0.61\bar{q})(1-\xi^2)$$

$$\mu_3 = \frac{1}{2}(1 + 0.61\bar{q} - 0.61\bar{\epsilon}) + \frac{1}{2}(\bar{\epsilon} - 1 - 0.61\bar{q} + 0.61\bar{\epsilon})(1-\xi)^2$$

$$\mu_4 = \frac{1}{2}(1 + 0.61\bar{q} - 0.61\bar{\epsilon}) + \frac{1}{2}(\bar{\epsilon} - 1 - 0.61\bar{q} + 0.61\bar{\epsilon})(1-\xi^2)$$

$$\xi = z_c / z_B$$

$z_c$ : height of the stratus cloud base

$(F_h)_s$ and $(Fq_w)_s$ mean $F_h$ and $Fq_w$ at the surface. From (8.16), (8.17), (8.18) and (8.19), we obtain the following budget equation of turbulent kinetic energy in the PBL,

$$\rho E q_m^2 = a_1 \rho u_*^3 + a_2 \rho \mid \Delta \mathbf{v} \mid^3 + \frac{g z_B}{\bar{s}_v}(A - \rho BE) - \rho \left(\delta + \frac{D q_m^2}{Dt}\right) z_B \tag{8.20}$$

Fig. 8.2 schematically summarizes the above relation. The last term in (8.20) may be proportional to the energy generation terms. Thus we assume

$$\rho \left(\delta + \frac{D q_m^2}{Dt}\right) z_B = a_3 \rho u_*^3 + a_4 \rho \mid \Delta \mathbf{v} \mid^3 + a_5 \frac{g z_B}{\bar{s}_v} \mathrm{Max}(A, 0) + \rho \delta_0 z_B \tag{8.21}$$

with adding possible background dissipation rate $\delta_0$ as suggested by Kim (1976). The term A may be negative, especially at night. As negative A means the destruction of turbulent kinetic energy, we set the term zero in that case. We introduce the representative turbulent kinetic energy $q_m^2$ within the PBL in deriving (8.20). We assume, following Randall (1976), that $q_m^2$ is a linear combination of $u_*^2$, the representative value of the purely dynamical boundary layer, and $w_*^2$, the representative value of the thermodynamical boundary layer defined by

$$w_*^3 = \max\left(0, \frac{g}{\bar{s}_v} \int_0^{z_B} \overline{w's_v'} dz\right), \tag{8.22}$$

*i.e.*,

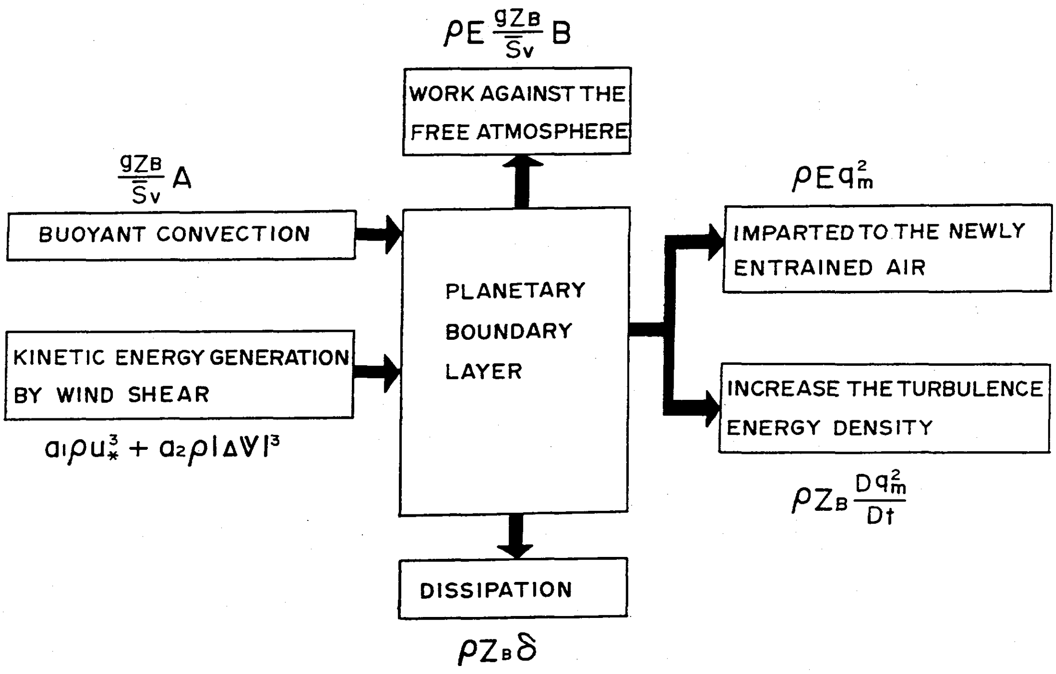


Fig. 8.2 Schematical figure of turbulent kinetic energy budget of the PBL. See text for details.

Table 8.1 Entrainment velocity experimentary determined under different situations.

| Case | Entrainment Velocity | Investigator |
|---|---|---|
| Very Unstable PBL With Strong Inversion | $E=0.2F_{sv}(0)/\rho\Delta_{sv}$ | Betts (1973) and others |
| Very Unstable PBL With Weak Inversion | $E=0.27w_*$ | Deardorff (1974) |
| Stable PBL With Strong Inversion | $E=2.5u_*^3/\frac{gZ_B}{\bar{S}_v}\Delta s_v$ | Kato and Phillips (1969) |
| Stable PBL With Weak Inversion | $E=0.28u_*$ | Lundgren and Wang (1973) |
| Stable PBL With Strong Wind Gap and Strong Inversion | $E=0.001\mid\Delta V\mid^3/\frac{gZ_B}{\bar{S}_v}\Delta s_v$ | Stull (1976) |

$$q_m^2 = b_1 w_*^2 + b_2 u_*^2. \tag{8.23}$$

where $b_1$ and $b_2$ are yet undetermined constants. In the daytime, $w_*^2$ is usually larger than $u_*^2$, *i.e.* $q_m^2 = b_1 w_*^2$. While in the night time, $q_m^2 = b_2 u_*^2$ because usually $w_*^2 = 0$. If we substitute the assumptions (8.21) and (8.23) into (8.20), the resultant equation has five constants yet undetermined, $a_1 - a_3$, $a_2 - a_4$, $a_5$, $b_1$ and $b_2$. These constants can be determined based on observations and laboratory and numerical experiments. Table 8.1 summarizes studies, adopted for determining those constants. The resulting equation is expressed as

$$E = \frac{2\frac{g z_B}{\rho \bar{s}_v} A - 2 w_*^3 + 2.5 u_*^3 + 0.001 \mid \Delta \mathbf{v} \mid^3 - 2\delta_0 z_B}{2\frac{g z_B}{\bar{s}_v} B + 1.85 w_*^2 + 8.92 u_*^2} \tag{8.24}$$

Currently the terms proportional to $\mid \Delta \mathbf{v} \mid^3$ and the background dissipation are dropped, because both terms still include some numerical uncertainties.

Turbulent fluxes at the surface are given by the bulk method based on similarity theory of turbulence in the surface layer. Many workers (Businger *et al.*, 1971 ; Yamada, 1976, *etc.*) have now shown that the bulk method is extended to include outer boundary layer. In the latter bulk method, the surface fluxes may be written,

$$\begin{aligned} (F_s)_s &= \bar{\rho} \mid \mathbf{v}_m \mid C_H C_D (s_g - s_m) \\ (F_q)_s &= \beta \bar{\rho} \mid \mathbf{v}_m \mid C_H C_D (q^*(T_g) - q_{wm}) \\ \mid \tau_s \mid &= \bar{\rho} C_D^2 \mid \mathbf{v}_m \mid^2 = \bar{\rho} u_*^2 \end{aligned} \tag{8.25}$$

$s_g$ is the dry static energy of the earth's surface, $\beta$ is an efficiency factor of evaporation and is a function of ground wetness (see Chapter 10), $C_H$ and $C_D$ are transfer coefficients of heat and momentum. $s_m$ and $q_{wm}$ are the representative values of s and $q_w$ within the PBL, and not the values at the surface. As for $C_H$ and $C_D$, Deardorff's value (1972) shown in Fig. 8.3 is adopted. They depend both on the bulk Richardson's number $Ri_B$ and the depth of the PBL normalized by the surface roughness length $z_0$ (see (10.1)). $Ri_B$ is given by

$$Ri_B = -\frac{g z_B (s_{vg} - s_{vm})_e}{c_p T_s \mid \mathbf{v}_m \mid^2} \tag{8.26}$$

$(s_{vg} - s_{vm})_e$ indicates effective difference of virtual static energy to estimate buoyancy flux

$$Fs_v = \begin{cases} Fs + \epsilon L\ (0.61 Fq - F_l) & : \text{outside clouds} \\ (1+\gamma)\alpha Fs - \epsilon L\ Fq_w & : \text{within clouds} \end{cases} \tag{8.27}$$

and is given by

$$(s_{vg} - s_{vm})_e = \begin{cases} (s_g - s_m) + 0.61 \epsilon \beta\ L(q^*_g - q_{wm}) & : \text{outside clouds} \\ (1+\gamma)\ (s_g - s_m) - \epsilon \beta\ L(q^*_g - q_{wm}) & : \text{inside clouds} \end{cases} \tag{8.28}$$

When the depth of the PBL increases, there may be more than one GCM layers in the

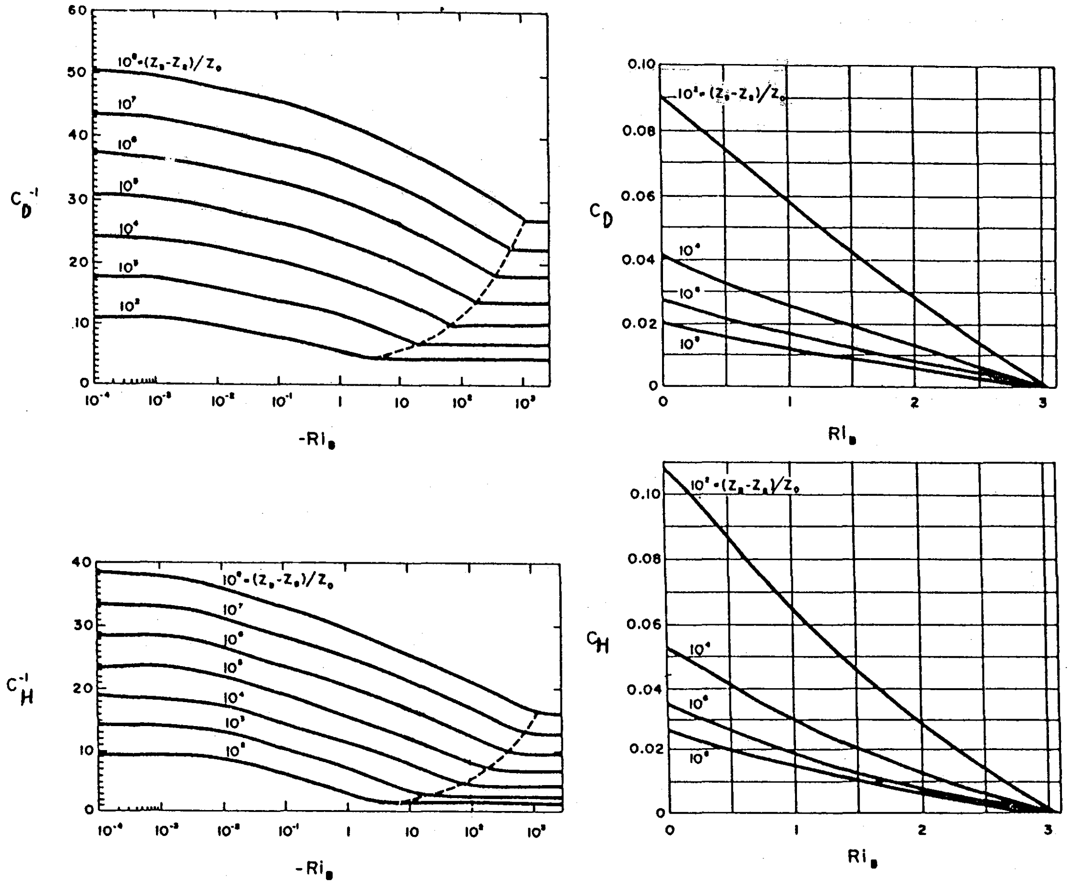


Fig. 8.3 Transfer coefficients $C_D$ and $C_H$ currently adopted. (Deardorff, 1972) Abscissa is the bulk Richardson number given by (8.26). Parameters are the depth of the PBL normalized with roughness length $z_0$.

PBL. In order to assure the fluxes of h, $q_w$ and $\mathbf{v}$ to be in the down-gradient direction, additional fluxes are added besides the linear vertical profile terms, *i. e.*,

$$F_h=(F_h)_B+((F_h)_s-(F_h)_B)\cdot\frac{\sigma-\sigma_B}{\delta\sigma_m}+K\frac{(\sigma-\sigma_B)(1-\sigma)}{\delta\sigma_m{}^2}\frac{\partial h}{\partial p}$$

$$Fq_w=(Fq_w)_B+((Fq_w)_s-(Fq_w)_B)\cdot\frac{\sigma-\sigma_B}{\delta\sigma_m}+K\frac{(\sigma-\sigma_B)(1-\sigma)}{\delta\sigma_m{}^2}\frac{\partial q_w}{\partial p} \qquad (8.29)$$

$$\mathbf{F}_v=(\mathbf{F}_v)_B+((\mathbf{F}_v)_s-(\mathbf{F}_v)_B)\cdot\frac{\sigma-\sigma_B}{\delta\sigma_m}+K_m\frac{(\sigma-\sigma_B)(1-\sigma)}{\delta\sigma_m{}^2}\frac{\partial \mathbf{v}}{\partial p}$$

$K=Km=18\ kg^2m^{-3}s^{-3}$ is currently adopted.

### 8.4 Stratus layer

We describe here a diagnostic determination of the stratus layer and its stability. Vertical profiles of the mixing ratio of total water substance $q_w$ is determined in a similar manner as is described in 8.5. At first, saturation condition is checked at $\sigma=\sigma_B$. If $q_w(\sigma_B)>q^*(\sigma_B, T_B)$, then stratus is assumed within the PBL. The mixing ratio of liquid water at $\sigma=\sigma_B$, $l_B$, is then determined. Secondly, the cloud base is determined based on the known distribution of $T(\sigma)$ and $q_w(\sigma)$.

When the PBL is capped with stratus, the stability of the stratus layer against the entrainment should be checked, because very dry air parcel entrained from above into the stratus may suffer negative buoyancy due to cooling and moistening through evaporation from the stratus.

When the PBL is cloud-free, the buoyancy gap at the top of the PBL, $\Delta s_v$, and the buoyancy flux there are

$$\Delta s_v=\Delta h-(1-0.61\epsilon)L\Delta q_w \tag{8.30}$$

$$(Fs_v)_B=-E\Delta s_v \tag{8.31}$$

If $\Delta s_v$ is negative, $(Fs_v)_B$ is positive and the rapid growth of the PBL depth may result. If $\Delta s_v<0$ happens in the model, the PBL is renewed, currently, to the shallowest possible condition with no gaps in physical variables at its top. 5mb is assigned as the shallowest possible depth of the PBL.

For a cloud-topped PBL, the stability condition becomes complicated because the evaporation of cloud must be considered in the stability analysis. $\Delta s_v$ and $(Fs_v)_B$ in a cloud-topped case are

$$\Delta s_v=\Delta h-(1-1.61\epsilon)L\Delta q-\epsilon L\Delta q_w \tag{8.32}$$

$$(Fs_v)_B=\alpha(F_h)_B-\epsilon L(Fq_w)_B=-E(\alpha\Delta h-\epsilon L\Delta q_w)+\alpha\Delta R \tag{8.33}$$

where use has been made of (8.6) and (8.7). (8.33) is transformed into

$$\left.\begin{aligned}&(Fs_v)_B=-E(\Delta s_v-(\Delta s_v)_{crit})+\alpha\Delta R\\ &(\Delta s_v)_{crit}=\frac{1-1.61\epsilon}{1+\gamma}L\cdot(q^*_{B^+}-q_{B^+})\end{aligned}\right\} \tag{8.33*}$$

where use has been made of the relation

$$L\Delta q=L\Delta q^*-L(q^*_{B^+}-q_{B^+})=\frac{1}{1+\gamma}[\gamma\Delta h-L(q^*_{B^+}-q_{B^+})]$$

(8.33)* shows that $(\Delta s_v)_{crit}$ is positive and is a measure of the relative humidity of the air above the stratus layer. When $\Delta s_v < (\Delta s_v)_{crit}$, entrainment tends to make $(Fs_v)_B$ positive. This helps to supply turbulent energy to the entrained air, causing large entrainment, rapid vertical mixing and evaporation of the layer cloud. This type of stability was pointed out first by Arakawa (1975) as the cause of transition from the stratus regime into the cumulus regime, and the criterion explained above was derived by Randall (1980) and Deardorff (1980). Currently, when $\Delta s_v < (\Delta s_v)_{crit}$ occurs in the model, the PBL is renewed to the shallowest possible condition with no gaps in physical variables at its top.

$\Delta R$ is a gap in the net upward radiative flux at the PBL top. When cloud is free, $\Delta R = 0$. While stratus clouds occupy the upper portion of the PBL,

$$\Delta R = 55 \cdot \mathrm{Min}\ (1.,\ \delta p_{stratus}/12.5)\ (\mathrm{W/m^2})$$

is assumed. $\delta p_{stratus}$ is the depth of the stratus layer in mb.

## 8.5 Vertical structure of the PBL model and the interpolation scheme

Fig. 8.4 illustrates the vertical structure of the discrete model. Let KB be the vertical index of the GCM layer which contains the PBL top at each grid point, at each time step. The layer KB is divided into two sublayers; layer P lies between $\sigma = \sigma_B$ and $\sigma = \sigma_{KB+1}$, while layer E lies between $\sigma = \sigma_{KB-1}$ and $\sigma = \sigma_{B^+}$. The depths of these layers are $\delta\sigma_p$ and $\delta\sigma_E$, respectively.

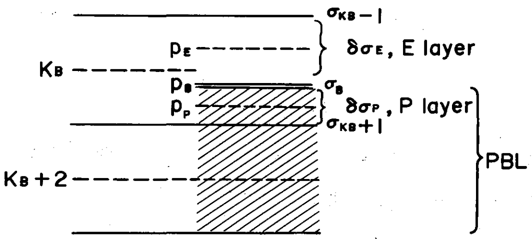


Fig. 8.4 Vertical indices related to the PBL.

Let $\psi$ be u, v, T or $q_w$. We define $\psi_k$(k: odd), $\psi_p$ and $\psi_E$ as;

$$\psi_k = \frac{1}{\delta\sigma_k}\int_{\sigma_{k-1}}^{\sigma_{k+1}} \psi d\sigma,\quad \psi_p = \frac{1}{\delta\sigma_p}\int_{\sigma_B}^{\sigma_{KB+1}} \psi d\sigma,\quad \psi_E = \frac{1}{\delta\sigma_E}\int_{\sigma_{KB-1}}^{\sigma_{B+}} \psi d\sigma \tag{8.34}$$

Then it follows that

$$\delta\sigma_{KB}\psi_{KB} = \delta\sigma_E\psi_E + \delta\sigma_p\psi_p \tag{8.35}$$

and

$$\delta\sigma_m\psi_m = \delta\sigma_p\psi_p + \sum_{k=KB+2}^{K} \delta\sigma_k\psi_k \tag{8.36}$$

$\psi_E$, $\psi_p$ and $\psi_{KB}$ may be significantly different from each other as $\Delta\psi$ is not equal to zero in general. There may be three candidates for a prognostic variable of the PBL, *i.e.*, $\psi_p$ (or $\psi_E$), $\psi_m$ and $\Delta\psi$. However, $\psi_p$ is not suitable as a direct prognostic variable because the PBL top may move from one GCM layer to the other from one time to the next. The prediction of $\psi_m$ might cause numerical troubles in determining $\psi_p$ when $\delta\sigma_p \rightarrow 0$ (see (8.36)). Thus we have chosen $\Delta\psi$ as a prognostic variable.

In the following, we derive a method of determining $\psi_p$ and $\psi_E$ from $\Delta\psi$ and $\psi_K$. First we let $\psi_p$ be

$$\psi_p = I_\Delta \Delta\psi + \Sigma I_k \psi_k \tag{8.37}$$

(8.37) is transformed, with use of (8.35), into

$$\psi_{B^+} - \psi_B = L_P \psi_p + L_E \psi_E + \sum_{k \neq KB} L_k \psi_k$$

where

$$\begin{aligned} L_p &= -\frac{1}{I_\Delta}[I_{KB}(1-\xi)-1] \\ L_E &= -\frac{1}{I_\Delta} I_{KB}\xi \\ L_k &= -\frac{I_k}{I_\Delta} \quad (k \neq KB) \end{aligned} \tag{8.38}$$

$$\xi = \delta\sigma_E / \delta\sigma_{KB}$$

In order to determine L, we have to specify extrapolation form for $\psi_{B^+}$ and $\psi_B$. We introduce here a new variable

$$\Psi = \psi p^{-\beta} \tag{8.39}$$

so that the variation of $\Psi$ with respect to pressure is much less than that of $\psi$. $\Psi_{B^+}$ may be extrapolated as

$$\Psi_{B^+} = \Psi_E + (\Psi_E - \Psi_{KB-2})\delta\sigma_E / (\delta\sigma_E + \delta\sigma_{KB-2}) \tag{8.40}$$

and $\psi_{B^+}$ is given by

$$\psi_{B^+} = \{1 + \delta\sigma_E/(\delta\sigma_E + \delta\sigma_{KB-2})\} \left(\frac{p_B}{p_E}\right)^{\beta_{B^+}} \psi_E - \delta\sigma_E/(\delta\sigma_E + \delta\sigma_{KB-2}) \cdot \left(\frac{p_B}{p_E}\right)^{\beta_{B^+}} \psi_{KB-2} \tag{8.41}$$

$\beta_{B^+}$ is determined by

$$\beta_{B^+} = |\tilde{\beta}_{B^+} \cdot \beta_s|^{1/2}.\ \mathrm{sign}(\tilde{\beta}_{B^+}) \tag{8.42}$$

where

$$\tilde{\beta}_{B^+} = \ln(\psi_{KB-2}/\psi_{KB}) / \ln(p_{KB-2}/p_{KB}) \tag{8.43}$$

and $\beta_s$ is a standard value currently specified as

$$\beta_s = \begin{cases} 0.16 & \text{for} \quad \psi = T \\ 3.20 & \text{for} \quad \psi = q_w \\ 0.0 & \text{for} \quad \psi = u \text{ or } v \end{cases} \tag{8.44}$$

sign ($\tilde{\beta}_{B^+}$) is an operation to take the same sign as $\tilde{\beta}_{B^+}$.

$\Psi_B$ may be extrapolated as

$$\Psi_B = \Psi_p - \begin{cases} (\Psi_{KB+2} - \Psi_p)\delta\sigma_p/(\delta\sigma_{KB+2} + \delta\sigma_p) & KB<K \\ 0 & KB=K \end{cases} \tag{8.45}$$

thus

$$\psi_B = \begin{cases} [1+\delta\sigma_p/(\delta\sigma_{KB+2}+\delta\sigma_p)]\left(\frac{p_B}{p_p}\right)^{\beta_B}\psi_p - \delta\sigma_p/(\delta\sigma_{KB+2}+\delta\sigma_p)\cdot\left(\frac{p_B}{p_p}\right)^{\beta_B}\psi_{KB+2} & KB<K \\ \left(\frac{p_B}{p_p}\right)^{\beta_B}\psi_p \qquad KB=K \end{cases} \tag{8.46}$$

When KB<K, $\beta_B$ in (8.46) is determined by (8.42) but with $\tilde{\beta}_{B^+}$ replaced by

$$\tilde{\beta}_B = \ln(\psi_{KB}/\psi_{KB+2})/\ln(p_{KB}/p_{KB+2}) \tag{8.47}$$

When KB=K, and the PBL is thermally stable ($(F_h)_s<0$), we assume $\beta_B = \beta_s$. When KB=K and $(F_h)_s>0$,

$$\beta_B = \begin{cases} R/c_p & \text{for} \quad \psi = T, \text{ unsaturated} \\ R/c_p/(1+\gamma) & \text{for} \quad \psi = T, \text{ saturated} \\ 0 & \text{for} \quad \psi = q, u, v \end{cases} \tag{8.48}$$

The comparison of (8.38) with (8.41) and (8.46) gives us:

$$\left.\begin{aligned} & L_E = \{1+\delta\sigma_E/(\delta\sigma_E+\delta\sigma_{KB-2})\}\left(\frac{p_B}{p_E}\right)^{\beta_{B^+}} \\ & L_{KB-2} = 1 - L_E \\ & L_p = -\left(\frac{p_B}{p_p}\right)^{\beta_B} - \begin{cases} 0 & KB=K \\ \left(\frac{p_B}{p_p}\right)^{\beta_B}\delta\sigma_p/(\delta\sigma_{KB+2}+\delta\sigma_p) & KB<K \end{cases} \\ & L_{KB+2} = -1 - L_p \end{aligned}\right\} \tag{8.49}$$

As $I_\Delta$, $I_{KB}$ and $I_k$ ($k \neq KB$) are

$$\left.\begin{aligned} & I_\Delta = -\xi/(L_E(1-\xi) - L_p\xi) \\ & I_{KB} = L_E/(L_E(1-\xi) - L_p\xi) \\ & I_k = \xi L_k/(L_E(1-\xi) - L_p\xi) \end{aligned}\right\} \tag{8.50}$$

$\psi_p$ is determined with the help of (8.37) and (8.49). $\psi_E$ is now obtained from (8.41), or

$$\left.\begin{aligned}&\psi_E=\varepsilon_\Delta\Delta\psi+\Sigma\varepsilon_k\psi_k\\&\text{where}\\&\varepsilon_\Delta=(1-\xi)/(L_E(1-\xi)-L_p\xi)\\&\varepsilon_{KB}=-L_p/(L_E(1-\xi)-L_p\xi)\\&\varepsilon_k=-L_k(1-\xi)/(L_E(1-\xi)-L_p\xi)\end{aligned}\right\}\tag{8.51}$$

**8.6 Numerical procedures**

Numerical procedures of the PBL processes are summarized in this section. The depth of the PBL is predicted with (8.1), where E is given by (8.24) and $M_B$ is given by the cumulus model described in Chapter 7. The discretized form of the horizontal mass flux convergence within the PBL is identical to the one described in Chapter 6 (see Eq.(6.29)) with q replaced by $\delta\sigma_m$ and with the interpolation (6.30) and (6.31) for $\hat{q}_{i+1/2,j}$ replaced by

$$(\widehat{\delta\sigma_m})_{i+½,j}=\frac{1}{2}[(\delta\sigma_m)_{i+1,j}+(\delta\sigma_m)_{i,j}]\tag{8.52}$$

Gaps at the PBL top of temperature, total water substance and momentum are predicted by (8.12), (8.13) and (8.14), respectively. Currently underlined terms in those equations are neglected for simplicity. The time change of the momentum gap is calculated at the $\pi$-point where thermodynamic variables are defined (see Fig. 4.1). As u and v are defined on the staggered grids, the time change of the momentum gap at the u and v points are interpolated simply as

$$\left(\frac{\partial\Delta u}{\partial t}\right)_{i+½,j}=\frac{1}{2}\left[\left(\frac{\partial\Delta u}{\partial t}\right)_{i,j}+\left(\frac{\partial\Delta u}{\partial t}\right)_{i+1,j}\right]$$

$$\left(\frac{\partial\Delta v}{\partial t}\right)_{i,j+½}=\frac{1}{2}\left[\left(\frac{\partial\Delta v}{\partial t}\right)_{i,j}+\left(\frac{\partial\Delta v}{\partial t}\right)_{i,j+1}\right]$$

In evaluating a gap in the vertical gradient of $\psi$, *i. e.*, $\Delta\left(\frac{\partial\psi}{\partial\sigma}\right)$, the extrapolation scheme introduced in 8.5 is followed, *i. e.*,

$$\Delta\left(\frac{\partial\psi}{\partial\sigma}\right)=\pi\left[\Delta\left(\frac{\partial\Psi}{\partial p}p^\beta\right)+\frac{1}{p}\Delta(\beta\psi)\right]\tag{8.53}$$

where $\partial\Psi/\partial p$ is given by (8.40) and (8.45).

The vertical gradient of the vertical flux of $\psi$ at the PBL top, *i.e.* $(\partial F_\psi/\partial\sigma)_B$ is evaluated by (8.29) where $\partial\psi/\partial p$ is estimated in the way stated in section 8.5 and the fluxes both at the surface and the PBL top are determined as described in the last part of this section.

In determining the entrainment rate E, turbulent flux profiles are required. While, the profiles of the turbulent fluxes depend on E. Therefore both E and turbulent flux profiles are determined by iteration. The process is schematically shown in Fig. 8.5. After determining transfer coefficients $C_D$ and $C_H$ in terms of $Ri_B$ and the normalized depth of the PBL, the turbulent fluxes at the surface are given by (8.25). By giving the first guess of turbulent fluxes at the PBL top, the entrainment velocity is determined by (8.24). After this, turbulent fluxes at the PBL top are evaluated with the use of (8.6), (8.7) and (8.10). w* defined by (8.22) is calculated with the new profiles of turbulent fluxes given by (8.29). Convergence of the iteration is checked with the value of w*. Currently the number of iteration is allowed up to 10.

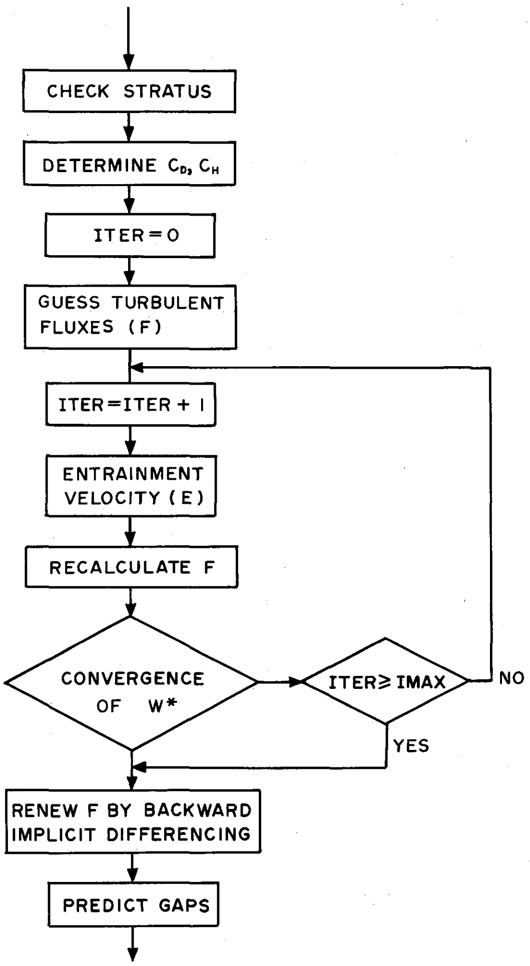


Fig. 8.5 Flow diagram of predicting gaps at the PBL top.

In the following, numerical procedure of determining turbulent fluxes are given based on backward implicit differencing (Randall, 1976). The need for this is to avoid linear computational instability in the course of rapid growth of gaps. Thermal energy fluxes are given by (8.6), (8.7) and (8.25). The first relation of (8.25) may be rewritten in terms of turbulent energy flux of moist static energy as follows;

$$\begin{aligned}(F_h)_S &= \mu_5 (F_s)_S + \mu_6 L (Fq_w)_S \\ &= \mu_5 V(s_g - s_m) + \mu_6 L \beta V(q_g - q_{wm})\end{aligned} \tag{8.54}$$

where

$$\mu_5 = \begin{cases} 1+\gamma_s & : \text{saturated (fog)} \\ 1 & : \text{otherwise} \end{cases}$$

$$\mu_6 = \begin{cases} 0 & : \text{saturated (fog)} \\ 1 & : \text{otherwise} \end{cases}$$

and $V = \bar{\rho}\,|\mathbf{v}_m|\,C_D C_H$. $\gamma_s$ is $\gamma = \frac{L}{c_p}\left(\frac{\partial q^*}{\partial T}\right)_p$ at the surface. Let $\tau$ be the time step with the time interval $\Delta t_d$ (see Fig. 5.1). Then (8.54), (8.25), (8.6) and (8.7) may be expressed as follows:

$$(F_h)_S^{\tau+1} = (F_h)_S^{\tau} + V\{\mu_5[c_p(T_g^{\tau+1} - T_g^{\tau}) - (s_m^{\tau+1} - s_m^{\tau})] + \mu_6 \beta L[(q_g^{*\tau+1} - q_g^{*\tau}) - (q_{wm}^{\tau+1} - q_{wm}^{\tau})]\} \tag{8.55}$$

$$(Fq_w)_S^{\tau+1} = (Fq_w)_S^{\tau} + \beta V[(q_g^{*\tau+1} - q_g^{*\tau}) - (q_{wm}^{\tau+1} - q_{wm}^{\tau})] \tag{8.56}$$

$$(F_h)_B^{\tau+1} = -E\Delta h^{\tau+1} + \Delta R = (F_h)_B^{\tau} - E(\Delta h^{\tau+1} - \Delta h^{\tau}) + (\Delta R^{\tau+1} - \Delta R^{\tau}) \tag{8.57}$$

$$(Fq_w)_B^{\tau+1} = (Fq_w)_B^{\tau} - E(\Delta q_w^{\tau+1} - \Delta q_w^{\tau}) \tag{8.58}$$

(8.55) ~ (8.58) are closed by introducing

$$s_m^{\tau+1} - s_m^{\tau} = \frac{g\Delta t_d}{\pi(\delta\sigma_m)^{\tau+1}}[(F_s)_S^{\tau+1} - (F_s)_B^{\tau+1}]$$

$$= \frac{g\Delta t_d}{\pi(\delta\sigma_m)^{\tau+1}}\left[\frac{1}{\mu_5}\left\{(F_h)_S^{\tau+1} - \mu_6(Fq_w)_S^{\tau+1}\right\} - \mu_7(F_h)_B^{\tau+1} + \mu_8 L(Fq_w)_B^{\tau+1}\right] \tag{8.59}$$

$$c_p(T_g^{\tau+1} - T_g^{\tau}) = \frac{c_p\Delta t_d}{C}[-(F_h)_S^{\tau+1} - R_6 - 4\sigma(T_g^{\tau})^3(T_g^{\tau+1} - T_g^{\tau}) + S_6^{\tau} + H_i^{\tau}] \tag{8.60}$$

$$\Delta h^{\tau+1} - \Delta h^{\tau} = -(h_m^{\tau+1} - h_m^{\tau}) = -\frac{g\Delta t_d}{\pi(\delta\sigma_m)^{\tau+1}}[(F_h)_S^{\tau+1} - (F_h)_B^{\tau+1}] \tag{8.61}$$

$$\Delta q_w^{\tau+1} - \Delta q_w^{\tau} = -(q_{wm}^{\tau+1} - q_{wm}^{\tau}) = -\frac{g\Delta t_d}{\pi(\delta\sigma_m)^{\tau+1}}[(Fq_w)_S^{\tau+1} - (Fq_w)_B^{\tau+1}] \tag{8.62}$$

where

$$\mu_7 = \begin{cases} \dfrac{1}{1+\gamma_B} & : \text{saturated (stratus)} \\ 1 & : \text{otherwise} \end{cases}$$

$$\mu_8 = \begin{cases} 0 & : \text{saturated (stratus)} \\ 1 & : \text{otherwise} \end{cases}$$

$\pi\delta\sigma_m$ is the depth of the PBL. (8.60) is derived from (10.10) and (10.11). C is the bulk heat capacity of the ground surface, $R_6$ is the net upward flux of terrestrial radiation, $S_6$ is the solar radiation absorbed at the ground surface, and $H_i$ is the upward heat conduction within the ground. With the help of (8.59)~(8.62), (8.55)~(8.58) are solved for $(F_h)_S^{\tau+1}$, $(F_h)_B^{\tau+1}$,$(Fq_w)_S^{\tau+1}$ and $(Fq_w)_B^{\tau+1}$. These fluxes are used for the prediction of gaps.

Momentum fluxes are renewed in a similar way. From the third equation of (8.25) and (8.10), we get

$$(\mathbf{F}_v)_S^{\tau+1} = (\mathbf{F}_v)_S^{\tau} - \frac{g\Delta t_d}{\pi(\delta\sigma_m)^{\tau+1}} \tilde{V}\left[(\mathbf{F}_v)_S^{\tau+1} - (\mathbf{F}_v)_B^{\tau+1}\right] \tag{8.63}$$

and

$$(\mathbf{F}_v)_B^{\tau+1} = (\mathbf{F}_v)_B^{\tau} + \frac{g\Delta t_d}{\pi(\delta\sigma_m)^{\tau+1}} E\left[(\mathbf{F}_v)_S^{\tau+1} - (\mathbf{F}_v)_B^{\tau+1}\right] \tag{8.64}$$

where $\tilde{V} = \bar{\rho} \mid \mathbf{v}_m \mid C_D^2$. $(\mathbf{F}_v)_S^{\tau+1}$ and $(\mathbf{F}_v)_B^{\tau+1}$ are obtained from (8.63) and (8.64).

**A 8.1 Some examples of the PBL model performance**

Some examples of time evolutions of the planetary boundary layer are shown in this appendix. All the examples are taken from the January simulation with the 5 layer tropospheric model. Data are sampled at four locations for two days. The locations are:

(0°, 22°N)···(This point is identified as "Sahara"),

(45°E, 80°S)···(This point is identified as "Mizuho"),

(180°, 6°N)···(This point is identified as "Equatorial Pacific"),

(95°E, 34°N)···(This point is identified as "Himalaya").

Fig. A8.1.1 (a) and (b) show time evolutions of the PBL at Sahara. $(\delta p)_B$ indicates the depth of the PBL in mb, $u_*$; the friction velocity in m/s, $\mid v \mid$; the mean wind speed within the PBL in m/s, $(F_h)_S$; the turbulent moist static energy flux at the surface in W/m², $T_S$; surface air temperature in K, $T_g$; ground surface temperature in K, $S_6$; the net downward flux of the solar radiation at the surface in W/m², $R_6$; the net upward flux of the terrestrial

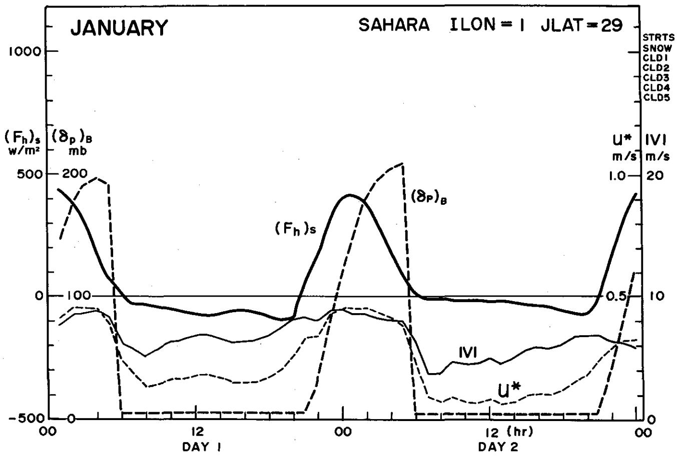


( a )

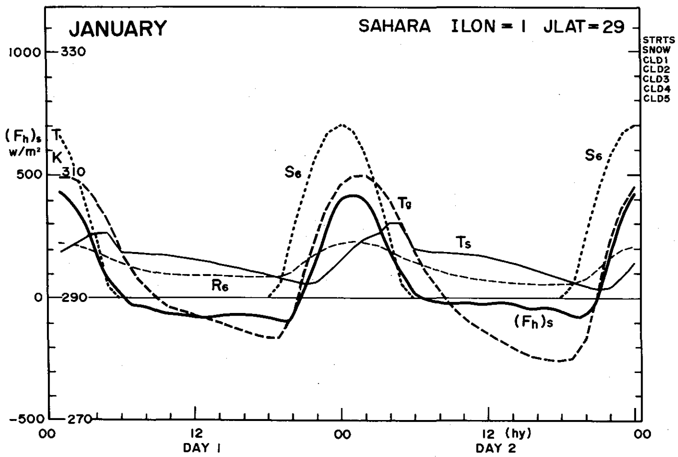


( b )

Fig. A8.1.1 Time change of variables related to the PBL at the grid point (0°, 22°N) identified as "Sahara". Data are taken from a January simulation with 5L -GCM.

(a) $(\delta p)_B$ is the depth of the PBL in mb ; $(F_h)_s$, upward turbulent flux of moist static energy at the surface ; $u_*$, friction velocity ; $|v|$, mean wind velocity in the PBL.

(b) $S_6$ is the solar flux absorbed at the surface ; $R_6$, the net upward flux of terrestrial radiation at the surface ; $T_s$, the surface air temperature ; $T_g$, the ground surface temperature.

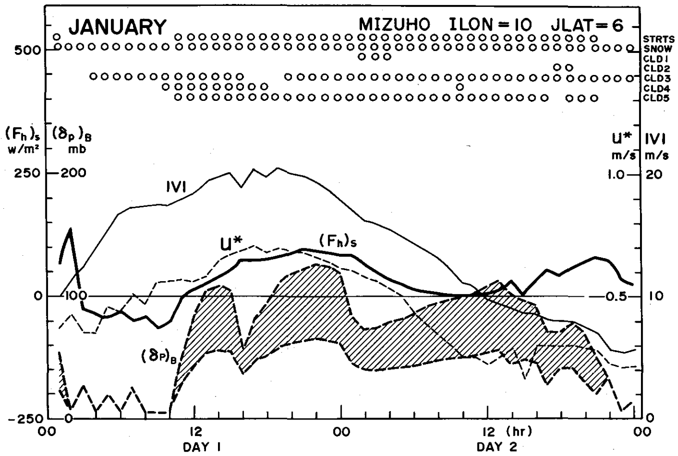


( a )

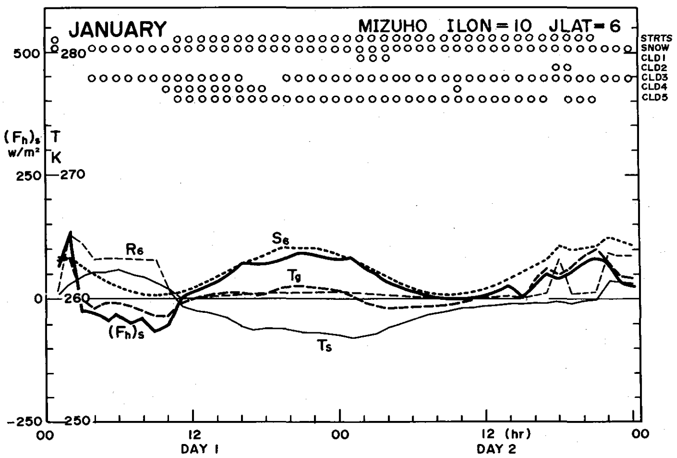


( b )

Fig. A8.1.2 Same as in Fig. A8.1.1 but for the grid point (45°E, 80°S) identified as "Mizuho". White circles in the upper part of the figure show the incidence of stratus, snow and large-scale clouds at each level. CLD5, for example, indicates clouds in the lowest (5th) level. Hatched area show the stratus layer.

radiation at the surface in $W/m^2$. A simple diurnal variation is seen in every field in Fig. A8.1.1. About 2 hours after sunrise, $(F_h)_s$ changes its sign from negative to positive. The rapid deepening of the PBL immediately follows the change. There is a sudden decrease of the PBL depth at the sunset. This is caused by the change of the sign of A in (8.19). It is interesting to note that the maximum $T_s$ occurs immediately before the sunset at this point.

Mizuho point is located in the Antarctica. The elevation is 1840m and the surface is covered with snow. Fig. A8.1.2 (a) and (b) show the time evolutions. Notations are the same as those used in Fig. A8.1.1. At the third (middle) and the fifth (lowest) levels exist clouds due to large scale condensation (see Chapter 9 and 13) most of the time. We can confirm that the increase in the net upward flux of the terrestrial radiation at the surface closely follows the disappearance of the lowest cloud. Around t=10hr of the first day, the surface air temperature starts to decrease probably due to large scale advection. The depth of the PBL starts to increase with the decrease of $T_s$, and the stratus is diagnosed within the PBL. Towards the end of the second day, the PBL depth decreases with the increase of $T_s$.

Fig. A8.1.3 (a) and (b) show the evolution at Equatorial Pacific. As the sea surface temperature ($T_g$) is almost constant and as no clouds appear during this period, $R_6$ is almost constant. It is commented that the variations of $R_6$ and $S_6$ do not directly influence the PBL over the ocean, because the sea surface temperature is given as external data in the present model. Roughly constant $(F_h)_s$ maintains the quasi-steady PBL. The positive $(F_h)_s$ is exclusively due to the upward water vapor flux as $T_g$ is less than $T_s$.

Fig. A8.1.4 (a) and (b) show the PBL evolution at Himalaya. This point is characterized with the high elevation (4329m). The surface is covered with snow. Therefore the maximum $S_6$ is only as much as 100 $W/m^2$. $R_6$ exceeds $S_6$ even during the daytime on the first day. The energy loss of the ground surface through radiation is compensated by negative $(F_h)_s$. Although friction velocity is relatively large, probably reflecting the high elevation, it is not enough to maintain thick PBL. During the last 9 hours of this period, the lowest level is covered with cloud. Corresponding to this change, $R_6$ decreases and changes its sign. There is also a net downward flux of solar radiation. Thus a rapid increase of the ground surface temperature occurs, causing the sign change of $(F_h)_s$.

Fig. A8.1.5 and A8.1.6 show global distributions of the PBL depth and the stratus incidence averaged over July. Shaded area in Fig. A8.1.5 shows the area where the depth is over 150 mb. Deep PBL exists over oceans, especially in the southern hemisphere around 30°S-60°S zone. It is difficult to verify present results against observations. Global features are

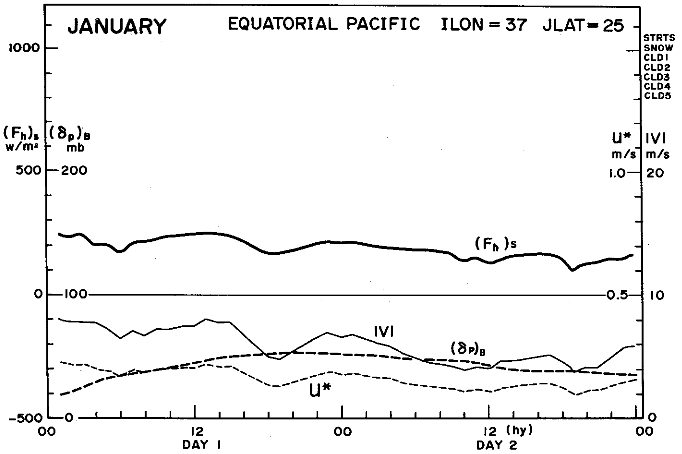


(a)

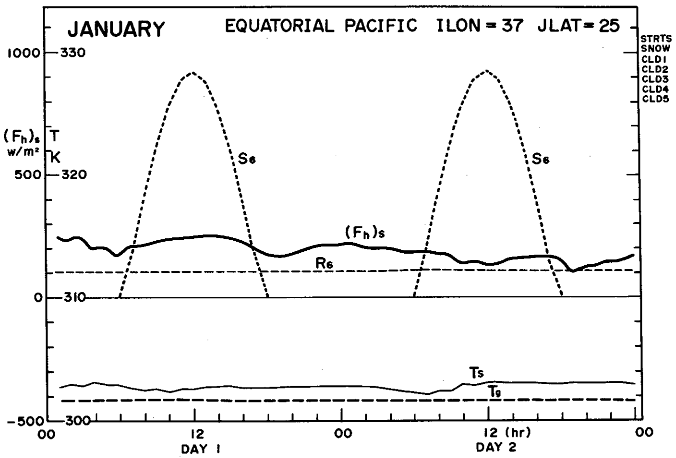


(b)

Fig. A8.1.3 Same as in Fig. A8.1.1 but for the grid point (180°, 6°N) identified as "Equatorial Pacific".

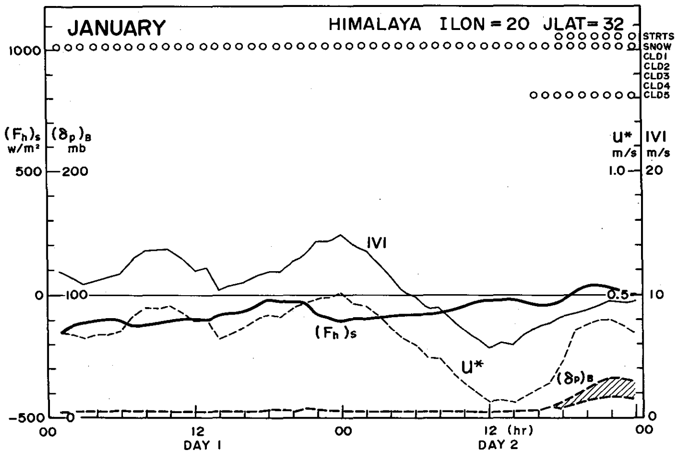


(a)

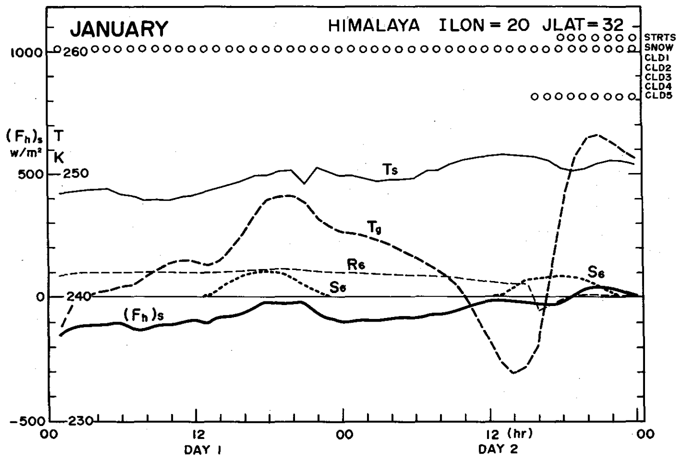


(b)

Fig. A8.1.4 Same as in Fig. A8.1.1 and Fig. A8.1.2 but for the grid point (95°E, 34° N) identified as "Himalaya".

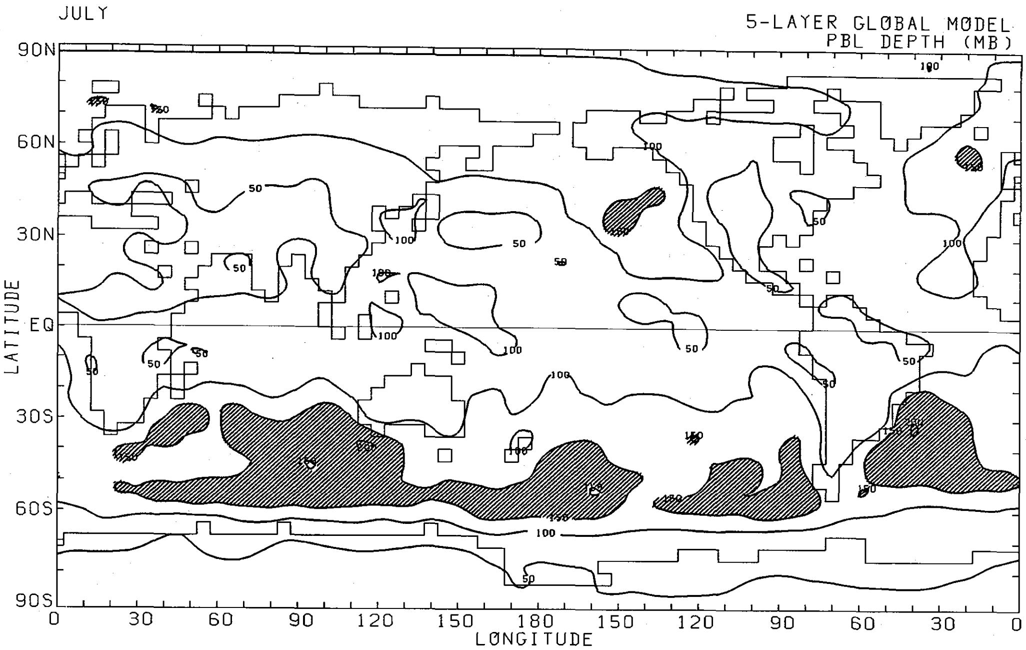


Fig. A8.1.5: : Global distribution of monthly mean depth of the PBL for July (unit: mb). The area where the depth is over 150mb is shaded.

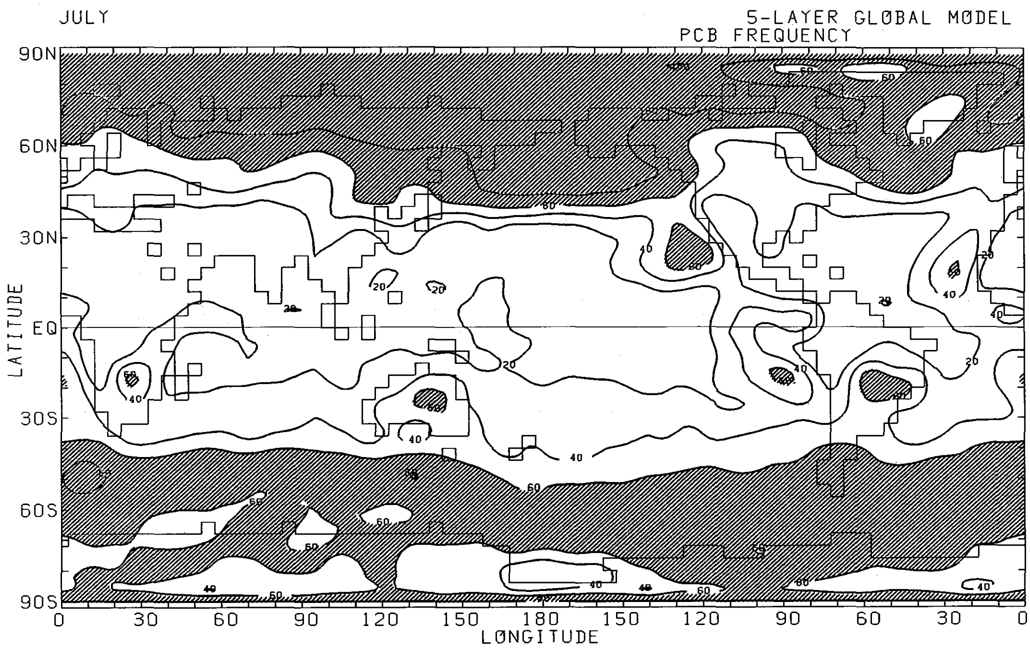


Fig. A8.1.6 : Global distribution of monthly mean stratus incidence for July in %. The area over 60% is shaded.

similar to the simulated results by Suarez, Arakawa and Randall (1983), although the PBL depth of the present model is almost twice as thick as that reported by Suarez *et al.*(1983).

Frequency of stratus incidence shown in Fig. A8.1.6 is high off the west coast of North America, South America, South Africa and North Africa. Shades indicate the acea where stratus occurs with the chance of 60% or more. Stratus incidence is also high over the Arctic Ocean as well as over the Antarctic Ocean. These areas correspond to the observed maxima of stratocumulus clouds, although further qualitative comparison has not been made. High stratus incidence over southern Africa has no counterpart in the observation. It is mentioned that this high incidence has a close connection to the wet ground surface condition there.